Journal of Power Sources 268 (2014) 853–860

Contents lists available at ScienceDirect

Journal of Power Sources

journal homepage: www.elsevier.com/locate/jpowsour

Proton dynamics in sulfonated ionic salt composites: Alternative membrane materials for proton exchange membrane fuel cells

N.E. De Almeida, G.R. Goward*

Department of Chemistry & Chemical Biology, McMaster University, 1280 Main St. West, Hamilton, ON L8S 4M1, Canada

HIGHLIGHTS

- Composite solid-acid membranes show H^+ conductivity under anhydrous conditions.
- Solid-state NMR reveals dynamics in composites relative to pristine solid-acids.
- NMR and impedance spectroscopy contrast local dynamics and conductivity.

ARTICLE INFO

Article history:
Received 10 February 2014
Received in revised form
12 May 2014
Accepted 17 May 2014
Available online 12 June 2014

Keywords:
Solid-acids
Ion transport
PEMFCs
^{1}H solid-state NMR
Composite materials

ABSTRACT

Hydrated Nafion, the most prevalent proton exchange membrane utilizes a vehicular mechanism for proton conduction. However, there is an increasing need for such membranes to perform under anhydrous conditions, at high temperatures, which would employ a structural transport mechanism for proton conductivity. Here, several solid-acids are characterized, both as pristine salts, and as polymer composites. Materials of interest include benzimidazolium methanesulfonate (BMSA), imidazolium methanesulfonate (IMSA), and imidazolium trifluoromethanesulfate (IFMS). The proton dynamics of these solid acids are characterized as pure salts, and as composites, embedded into porous Teflon, by solid state NMR. It was determined that spin lattice (T_1) relaxation of the composites are systematically lower than that of the pure salt, indicating that local dynamics are enhanced in the composites. Spin–spin relaxation (T_2^*) was measured as a function of temperature to determine the activation energy for local mobility for each salt and composite. The activation energy for local proton mobility in each salt decreased after being inserted into porous Teflon. Finally, the long-range ion transport was characterized using impedance spectroscopy. The IFMS–Teflon composite possessed the lowest activation energy for local proton mobility, the highest thermal stability, and the most favorable proton conductivity, among the investigated materials.

1. Introduction

Proton exchange membrane fuel cells (PEMFCs) are promising energy carriers for portable and automotive applications. Several limitations prevent widespread use of PEMFCs such as cost, lifetimes, and availability of infrastructure. PEMFCs which are able to operate at higher temperatures would prevent carbon monoxide poisoning of the platinum catalyst, and yield higher current densities [1–3]. Perfluorosulfonic acid ionomers such as Nafion are the most widely used PEMs due to their inherent durability, chemical stability and high proton conductivity. However, in contrast to optimal conditions for the platinum catalyst, Nafion operates optimally under humid, low temperature (<80 °C) conditions [4–6].

Nafion composites have been widely studied in literature [7,8]. A common approach is to add components to Nafion to enhance performance at higher temperatures by maintaining water within the membrane. Therefore, hygroscopic additives are inserted to enhance water retention properties under high temperature and low humidity conditions. Examples of additives include SiO_2 and TiO_2 which have been shown to maintain water content but do not contribute to proton conductivity [9–12].

Alternatively, electrolyte materials that can operate under anhydrous conditions would be ideal to mitigate water management issues. The mechanism of anhydrous proton transport has been studied by molecular dynamics simulations, and occurs through the Grotthuss mechanism [13,14]. A class of electrolytes

* Corresponding author. Tel.: +1 (905) 525 9140x24176; fax: +1 (905) 522 2509.
E-mail address: goward@mcmaster.ca (G.R. Goward).

http://dx.doi.org/10.1016/j.jpowsour.2014.05.150
0378-7753/

that fits these criteria is solid acids, which are chemically, thermally and electrochemically stable and transport protons under anhydrous conditions [15–18]. Research in this area first focused on $CsHSO_4$, however drawbacks were identified, including narrow operational temperature ranges and significant hydration difficulties [19,20]. Previously studied organic solid acids utilized phosphate functional groups, paired with large heterocyclic cations, where it was shown that these systems have good conductivity in anhydrous conditions [21]. Phosphates possess substantial proton conductivity; however high temperatures can promote their condensation into pyrophosphates. The resultant P–O–P linkages between neighboring phosphate groups decrease proton conductivity irreversibly [22]. In contrast, sulfonate functional groups are chemically, stable and have been used within membranes under harsh environments, such as fuel cells, with great success and do not condense at high temperatures.

In this paper sulfonate-functionalized solid acids were investigated. Solid acids were synthesized using organic heterocycles such as imidazole and benzimidazole, paired with sulfonic acid derivatives to form acidic salts. However, the salts themselves do not possess the mechanical properties necessary to be formed into thin films for fuel cell and require a polymer support to be relevant for fuel cell applications.

It has been shown that ionic salts can be incorporated into polymers to provide the necessary mechanical support [23]. One example of a polymer support is polyvinylidenefluoride (PVDF), however the salt does not insert homogenously into the host polymer causing numerous non-conductive pathways. Porous Teflon is an alternative host candidate which behaves similarly to PVDF, and when the salt was inserted a homogenous film was obtained [24]. The properties of the sulfonic acid salts, and their Teflon-composites are investigated here using a series of ^{1}H solid-state nuclear magnetic resonance (SSNMR) experiments, paired with impedance spectroscopy measurements of the proton conductivity.

2. Methodology

Solid state NMR is capable of probing dynamics on a localized scale. In the solid state broad ^{1}H line widths are expected due to the strong homonuclear dipole–dipole interactions, arising from the lack of molecular rate in solid samples [25]. Dipole–dipole interactions are based on the gyrometric constant (γ_i and γ_j) of the relevant nuclei (I_i, and I_j) and the distance (r) and orientation (θ) between them as seen in Equation (1), where the Hamiltonian for the dipolar interaction, H_D, includes two spatially dependent terms, and a third, spin-dependent term [26]. The first two terms are based on constants, and together form the dipolar coupling constant, D_{ij}.

$$H_D = \frac{\left(\frac{\mu_o}{4\pi}\right)\hbar\gamma_i\gamma_j}{r_{ij}^3}\left(3\cos^2\theta - 1\right)\left(\frac{3I_{iz}I_{jz} - \widehat{I}_i\widehat{I}_j}{2}\right) \quad (1)$$

Dipole–dipole interactions can be averaged with the use of fast magic angle spinning (MAS), which generates significant line narrowing. However by averaging these effects valuable structural information is removed. In particular, the strength of the dipole–dipole couplings can be used to determine the relative mobility of protons in a hydrogen-bonded structure. Therefore, selectively retrieving these couplings can provide unique, site-specific insight into the local dynamics. Pulse sequences such as *Back to Back* (BaBa) are used to recouple homonuclear dipole–dipole coupling over the timescale of the rotor period [27,28]. Strong dipole–dipole couplings will be fully excited on timescale of 2τ, where τ is equal to the rotor period (25 kHz = 40 μs), whereas the signals of mobile protons will be attenuated or removed from the spectrum due to the inefficient excitation of the double-quantum coherence. In this sense, only strongly dipolar coupled signals pass through the double quantum filter (DQF). It is important to note that the lack of a DQ signal can be attributed to either to fast molecular tumbling (averaging θ or r) or long distance (r) between the protons. Therefore, the DQ data presented here are evaluated for the relative mobility, keeping in mind the crystal lattice, and density of protons within each structure.

Spin lattice relaxation (T_1) has several different mechanisms such as dipolar, scalar, quadrupolar and chemical shift anisotropy. In this case it is assumed that dipolar relaxation is the dominate mechanism that contributes to spin lattice relaxation [29]. Investigation of salts and salt-composites will be performed here, and a change in spin lattice relaxation will be interpreted as indicative of dipole–dipole coupling changes. This interpretation is valid for the protons in these materials, as there are negligible quadrupolar or chemical shielding anisotropy interactions present.

Variable temperature (VT) MAS NMR is a routinely used technique to probe dynamics at a molecular scale. To establish linewidth trends, the full width half max (FWHM) of the individual peaks are determined. The T_2^* can be calculated, from FWHM (Equation (2)), and is indicative of T_2 relaxation coupled with the effect of field inhomogeneity [30,31]. The behavior of T_2^* as a function of temperature follows an Arrhenius relationship, and can be used to estimate the activation of proton mobility on a localized scale.

$$\mathrm{FWHM} = 1/\pi T_2^* \quad (2)$$

Additionally, in fast exchange the chemical shift is observed trend to lower ppm values with increasing temperature. In this case, the higher thermal energy in hydrogen bonded network causes less electron shielding at the ^{1}H nucleus, and thereby lowers chemical shift [28,32].

While ^{1}H NMR provides a local picture of the dynamics in the hydrogen bonding motif, proton conductivity is more frequently obtained *via* electrochemical impedance spectroscopy (EIS), which probes the bulk transport properties [33]. Measurements are conducted with an in-plane (composites) or through-plane (salts) conductivity cell to determine the impedance of a sample and thus its conductivity [33,34]. This is a macroscale measurement of the performance of a material as an electrolyte for fuel cell systems. Conductivity measurements can be correlated with NMR data to describe the mechanism of proton transport within the composites [21].

3. Experimental

Benzimidazolium methanesulfonate (BMSA) and imidazolium methanesulfonate (IMSA) were synthesized by dissolving benzimidazole or imidazole in minimal amounts of methanol and adding methanesulfonic acid to maintain a 1:1 molar ratio. The solution was left to crystallize the product. Crystals were heated at 80 °C oven for 24 h to remove any trapped solvent. Imidazolium trifluoromethanesulfonate (IFMS) was purchased from Sigma Aldrich. Porous Teflon film was purchased from Millipore with 0.45 μm pores and 47 μm in thickness. To produce composites porous Teflon was soaked in a salt solution for 24 h. IMSA and IFMS were made into 1 M salt solutions and the BMSA was made into a 0.5 M salt solution due to solubility limitations. The composite was placed into an 80 °C oven for 24 h. The salts are referred to by their acronyms and the corresponding composites as, for example,

BMSA–Teflon, indicating the salt embedded in the Teflon membrane.

Differential scanning calorimetry was performed on a Mettler Toledo FP90 TA Cell heating 20 °C min^{-1} from 30 °C to 300 °C under atmospheric conditions. Heat flow was calibrated using indium metal. All samples were packed into aluminum pans with approximately 10 mg of material before placing into instrument. Thermogravimetric analysis (TGA) was performed on a NETZSCH STA 409 PC/PG instrument referenced with Al_2O_3 with a 10 °C temperature ramp from 35 °C to 700 °C under air.

NMR experiments were performed on a Bruker Avance 500 spectrometer, equipped with an 11.7 T magnet. All samples were referenced to adamantane (1.85 ppm for ^1H) [35]. For salt samples NMR was conducted with a 2.5 mm diameter rotor spinning at 25 kHz. Solid state ^1H NMR spectra were acquired with a 90° pulse length of 2.5 μs. Delays set were chosen to be 5 times greater than the T_1 of the sample. T_1 measurements were obtained using a saturated recovery method [36]. Composite samples were measured with a 4 mm diameter rotor spinning at 10 kHz. Solid state ^1H NMR spectra were acquired with a 90° pulse length of 5 μs. Fitting of the NMR peaks to determine their full width half max (FWHM) was performed in Mathematica (Version 8) [37].

Double quantum experiments were obtained with the back to back sequence (BaBa). Experiments were performed on a 2.5 mm rotor spinning at 25 kHz that was rotor synchronized for 2τ (80 μs periods). Experiments were collected with 16 scans to complete the full phase cycle.

Variable temperature bearing gas was heated for all variable temperature experiments and conducted in the 300–350 K range. Temperatures were calibrated using a $SmSn_2O_7$ temperature calibration [38].

Single crystal X-ray experiments were obtained by first dissolving the salt in saturation in methanol. All crystals obtained were clear and colorless. X-ray diffraction measurements were conducted with Bruker D8 diffractometer with a SMART6000 CCD detector. The radiation source was a Cu K-α with a wavelength of 1.54178 Å.

Electrochemical impedance spectroscopy was obtained on a Gamry Reference 600 potentiostat. Pure salts were pressed into pellets, sintered at 130 °C overnight and covered in a 30 nm of gold on both sides for through-plane conductivity measurements. Composites samples were analyzed using an in-plane conductivity cell. The samples were cut into 0.5 × 2 cm to be placed into the conductivity cell. The cell was placed in an oven with anhydrous conditions to equilibrate for 1 h before proton conductivity measurements with a temperature range of 80 °C–120 °C. Experiments were conducted at a DC voltage of 0.5 V with amplitude of 50 mV with frequency sweep from 1.0×10^6 to 1.0×10^3 for pure salts and 1.0×10^5 to 1 Hz for composites.

4. Results

Producing anhydrous salt-host composite for fuel cells would be beneficial to increase the longevity of the catalyst layer, enhance proton conductivity and minimize water issues within the cell. Sulfonated salts were investigated by themselves and within a Teflon host for the applicability as an electrolyte for fuel cell applications. Here these salts and composites were studied on a molecular scale by solid state NMR to observe proton mobility. This information can be used to explain how the proton conductivity is affected by the hydrogen-bonded network within the salts and composites.

4.1. Single crystal X-ray diffraction

Single crystal X-ray diffraction was performed to identify the H^+ transport pathways by fully describing the hydrogen bonding motifs, unit cell coordinates and space group. The resulting structural data, including space group unit cell parameters are reported in Fig. 1 and Table 1. As seen in Fig. 1A the BMSA salt structure has two hydrogen bonds of the same length and the same local environment. The cation rotation may be inhibited, due the size of the heterocycle whereas the anion appears to have the ability to freely rotate, due to the labile nature of the two attached hydrogen bonds. Therefore, proton conduction is proposed to occur in this salt *via* the rotation of the anion. In contrast, as shown in Fig. 1B, the cation and the anion in the IMSA salt have space to freely rotate. In Fig. 1C the ions in the IFMS salt structure are spaced comparatively further apart, creating ample space for rotation of the cation. The anion experiences steric hindrance between the fluorinated methyl groups which may inhibit its reorientation. Only the sulfonate group appears spatially able to exhibit free rotation in IFMS; however it must break three hydrogen bonds in order to participate in proton conductivity. These structural constraints will be further considered in the context of the conductivity and local mobility, as assessed by solid state NMR.

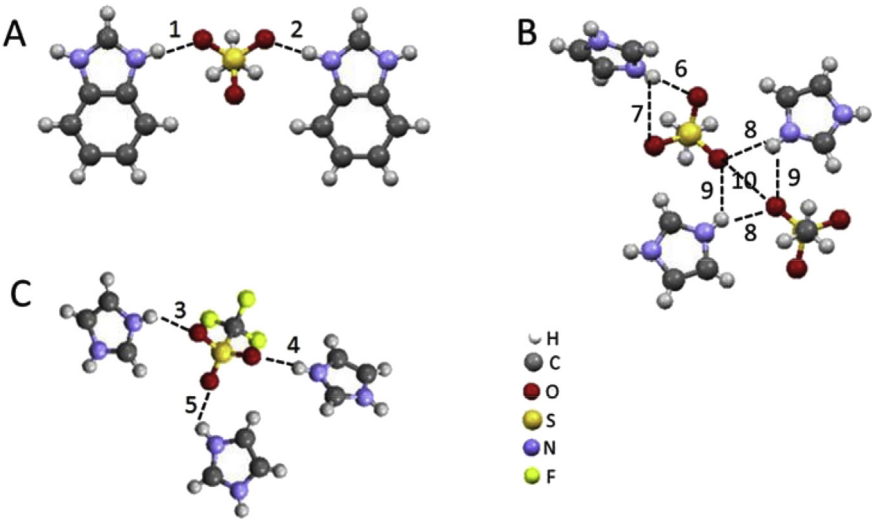

Fig. 1. Single crystal X-ray from saturated salt methanol solutions A) BMSA, B) IMSA and C) IFMS.

Table 1
Lengths of bonds for BMSA (space group: $P2_1\,2_1\,2_1$), IFMS (space group: $P4_3\,2_12$) and IMSA (space group: *Pbca*) single crystal X-ray.

Compound name	Bond number	Length (Å)	*a* (Å)	*b* (Å)	*c* (Å)
BMSA (A)	1	2.710(4)	5.665(3)	9.604(4)	18.096(9)
	2	2.701(4)			
IFMS (B)	3	2.841(3)	8.100(3)	8.100(3)	24.898(2)
	4	2.965(3)			
	5	2.837(3)			
IMSA (C)	6	2.802(2)	7.959(2)	11.038(3)	16.159(5)
	7	2.831(2)			
	8	2.842(2)			
	9	3.045(2)			
	10	3.049(2)			

4.2. Thermogravimetric analysis

The structures of the three solid-acids of interest are shown in Fig. 1, as excerpts from the crystal structures. Initial analysis of the BMSA, IMSA and IFMS, salts was performed with DSC. The melting points for BMSA, IMSA and IFMS were determined to be 240 °C, 191 °C, and 189 °C respectively. Based on the relative melting points, IFMS was predicted to show an onset of proton dynamics at the lowest temperature. For salt–polymer composite samples, salt loadings were determined by TGA. It was found that the salt loadings for BMSA–Teflon, IMSA–Teflon and IFMS–Teflon, and were 28%, 34% and 44% respectively as seen in Fig. 2. The salt loadings are not equivalent for the three composites due solubility limits of each salt in methanol. Teflon swells in methanol allowing the pores to expand to host the salt in solution and remain in the pores when Teflon was dried resulting in a composite. Salts in the composites possessed a higher thermal stability than the salts themselves, as shown by the relative inflection points of the TGA curves. The inflection points for BMSA–Teflon, IMSA–Teflon and IFMS–Teflon, were 278 °C, 301 °C and 370 °C respectively. IFMS–Teflon possesses the highest salt loading and the highest thermal stability compared to the other salt–Teflon composites. Previous studies by Yan et al. investigated organic solid acids in Teflon composites with scanning electron microscopy (SEM) [24]. It was shown that the salt formed as a phase-separated microstructure that incorporated throughout the Teflon pores.

4.3. ^{1}H MAS NMR on salts

The ^{1}H MAS NMR spectra (above) and ^{1}H DQF NMR spectra (below) of the three compounds are shown in Fig. 3. Spectra were acquired at 25 kHz MAS, and exhibited no significant spinning sideband intensity. The spectra can be divided into three regions of interest; hydrogen-bonded (16–9 ppm), aromatic (9–5 ppm) and the aliphatic (5–0 ppm).

4.3.1. BMSA

In BMSA salt one hydrogen-bonded peak is observed at 13 ppm (A), three aromatic peaks at 8 ppm (B), 6 ppm (C) and 4 ppm (D) and one aliphatic proton at 3 ppm (E). Variable temperature NMR indicates dynamics at hydrogen-bonded peak, which narrows as a function of temperature (Fig. 4). The ^{1}H NMR spectra of the BMSA salt exhibit line narrowing as a function of temperature, indicative of local dynamics. The FWHM was correlated to T_2^* to determine the activation energy of proton mobility, which was 9.7 ± 0.1 kJ mol^{-1} as seen in Table 2.

Another approach to observe proton mobility was to perform a VT ^{1}H DQF NMR study. The ^{1}H DQF NMR data shown in Fig. 3 for BMSA none of the peaks are completely removed by the double quantum filter (under recoupling = $2\tau_r$), however they are attenuated significantly, relative to the direct-excitation spectrum, (over 90%) which is attributed to local mobility. As the temperature increased from 300 to 350 K the intensity from the hydrogen-bonded proton decreased substantially due to increasing mobility. This qualitative method to determine how the hydrogen-bonded proton attenuates compared with the attenuation of the aliphatic region. The relative degree of attenuation at the hydrogen-bonded proton, as compared to the other (covalently bound) protons was 30 ± 2% and 15 ± 2% respectively. Therefore, the hydrogen-bonded proton is inferred to possess a higher degree of mobility on a timescale of 80 μs. This statement is based on the assumption that the static (low temperature) homonuclear dipolar couplings for all protons in the structure would be approximately equivalent when summed over the proton-rich structure. Full simulation of the multi-spin-dynamics is beyond the scope of this study [39].

4.3.2. IMSA

The ^{1}H NMR spectrum of IMSA has four main proton resonances including the hydrogen-bonded peak at 13.0 ppm (A), the aromatic peaks at 7.6 ppm (B) and 9.1 ppm (C) and the aliphatic peak at 1.7 ppm (D) as seen in Fig. 5 [40]. The hydrogen-bonded peaks in IMSA and BMSA have equivalent chemical shifts, indicating similar environments around the protons. IMSA hydrogen-bonded and aromatic protons have attenuated the same degree and the aliphatic region attenuated by the greatest amount. A similar result was also observed by Traer and Goward [40]. This is typical of the rapidly rotating methyl groups, which are inherently decoupled through this mobility [41]. With VT ^{1}H MAS NMR the hydrogen-bonded proton shifts to lower frequency as expected, which is consistent with a Grotthuss mechanism of proton transport [42]. Additionally, the FWHM decreased as a function of temperature and the activation energy of proton mobility in IMSA was 7.4 ± 0.1 kJ mol^{-1}, which is lower than BMSA, consistent with the structural interpretation above. Also, with the ^{1}H DQF NMR VT the hydrogen-bonded proton attenuated significantly, a total of 68 ± 2%, whereas the aromatics were attenuated by only 10 ± 1%. Since the hydrogen-bonded proton attenuated significantly compared to the other protons in the system that it can be concluded it possesses higher degree of mobility. However, this degree of mobility could be due to a rapid local dynamics or a long range transport contributing to proton conductivity. To confirm whether this local mobility of the H-bonds leads to long range ion transport, the bulk ion transport properties are measured (below).

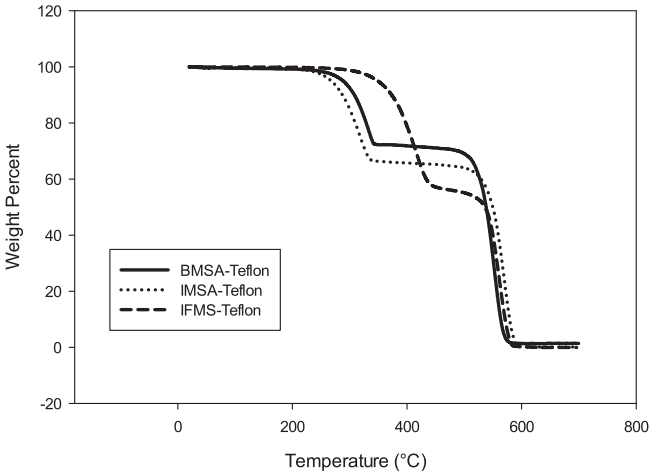

Fig. 2. TGA of BMSA–Teflon, IFMS–Teflon and IMSA–Teflon in air, 10 °C min^{-1} heating rate.

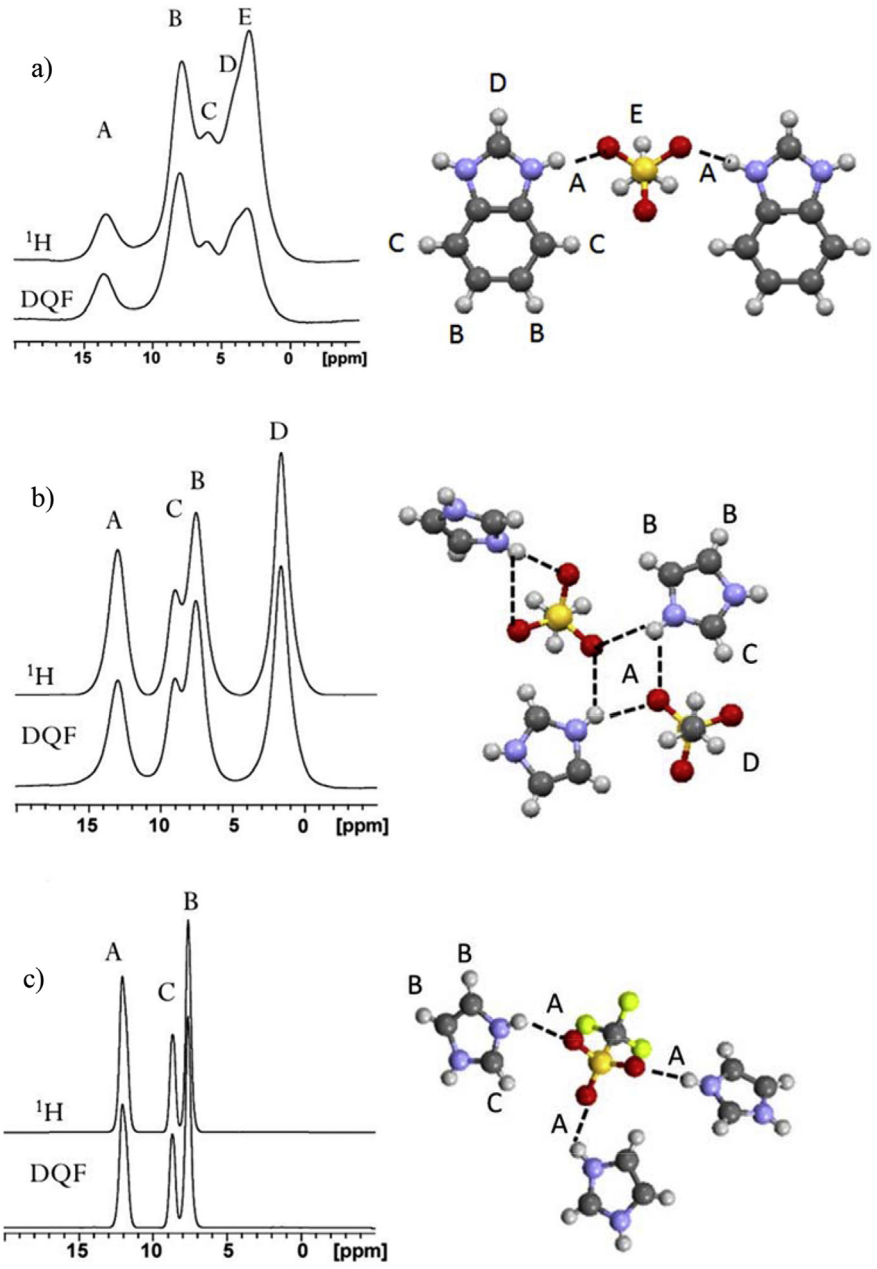

Fig. 3. ^{1}H MAS NMR spectra @ 25 kHz (4 scans) and ^{1}H DQF NMR (16 scans) of a) BMSA all peaks attenuate by the same degree b) IMSA hydroxyl peak has decreased intensity suggesting dynamics c) IFMS hydroxyl peak attenuates slightly more than remainder of peaks suggesting dynamics.

4.3.3. IFMS

The third structure of interest, IFMS has three protons shifts 11.4 ppm for the hydrogen-bonded peak (A), 8.1 ppm for the first aromatic proton (C) and 7.1 ppm for the second type of aromatic proton (B). The peaks in this spectrum are significantly narrower than BMSA and IMSA. This is attributed to the lower homonuclear ^{1}H–^{1}H dipole–dipole coupling in this fluorinated structure, relative to the others. Thus, IFMS has the most dilute homonuclear dipolar-coupling network of the salts considered here. In the variable temperature ^{1}H MAS NMR spectra, all the peaks narrow uniformly as a function of temperature as seen in Fig. 6. A correlation was determined for the T_2^* in an Arrhenius plot. The activation energy was the lowest of the three salts being 5.5 ± 0.6 s kJ mol^{-1} as seen in Table 2. In the ^{1}H DQF MAS NMR spectrum the protons have greatly attenuated in all regions suggesting either high mobility in all protons present or the absence of close neighbors (<3.5 Å) [43]. VT ^{1}H MAS NMR depicts the aromatic protons decreasing by 14 ± 1% and the hydrogen-bonded region by 19 ± 1%. This was not as a dramatic difference as the other salts however, since the dipole–dipole coupling with IFMS was small initially, large changes are not expected.

4.4. ^{1}H NMR of salt–Teflon composites

Further comparison was made in the ^{1}H MAS NMR spectra of the salt–Teflon composites, utilizing the relaxation properties of the salts, as compared to their composites, as a measure of the tightness of the local hydrogen-bonding networks. Spin lattice relaxation decreased from 5.5 ± 0.1 s, for the pure BMSA salt, to 4.5 ± 0.3 s for BMSA–Teflon composite, indicating that dipole–dipole

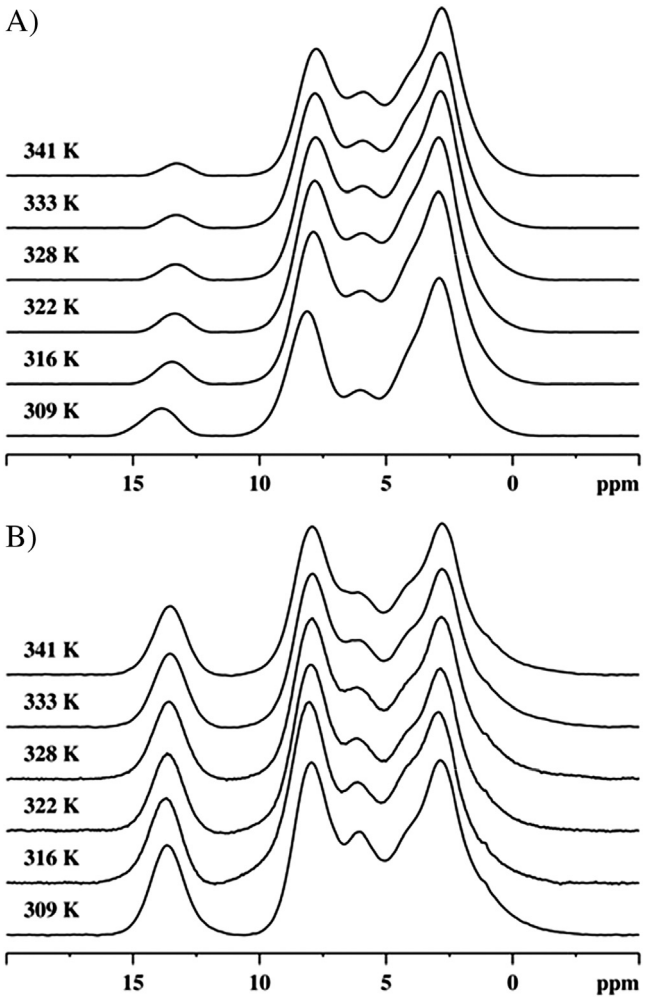

Fig. 4. VT ^{1}H MAS NMR, 25 kHz, 500 MHz, 2.5 mm probe A) BMSA salt and B) BMSA–Teflon composite.

interactions have decreased modestly from pure salt to composite (Table 3). This is supported with the change of activation energy from 9.7 ± 0.1 kJ mol^{-1} to 5.6 ± 0.2 kJ mol^{-1} for the BMSA salt and BMSA–Teflon respectively as seen in Table 2. Here, shortened T_2 relaxation times depicts higher local mobility, which is expected from the interaction between salt and Teflon, due to the lack of long-range crystallinity, imposed by the membrane pore structure. A shorted T_2^* relaxation does not uniquely imply more rapid proton-transport processes. Nevertheless, it was expected that additional dynamics would occur while inserted into the polymer support, as defects in the packing-structure are thought to enable Grotthuss-mechanism transport [44].

Table 2
Activation energies acquired from Arrhenius analysis of T_2^* and EIS data for IMSA, BMSA and IFMS salts and composites acquired under variable temperature ^{1}H MAS NMR.

Compound	Activation energy (kJ mol^{-1})	
	NMR	EIS
BMSA	9.7 ± 0.1	29.5 ± 1.5
IMSA	7.4 ± 0.1	21.2 ± 0.1
IFMS	5.5 ± 0.6	29.6 ± 0.8
BMSA–Teflon	5.6 ± 0.2	N/A
IMSA–Teflon	4.0 ± 0.1	29.8 ± 0.9
IFMS–Teflon	3.6 ± 0.2	21.4 ± 0.6

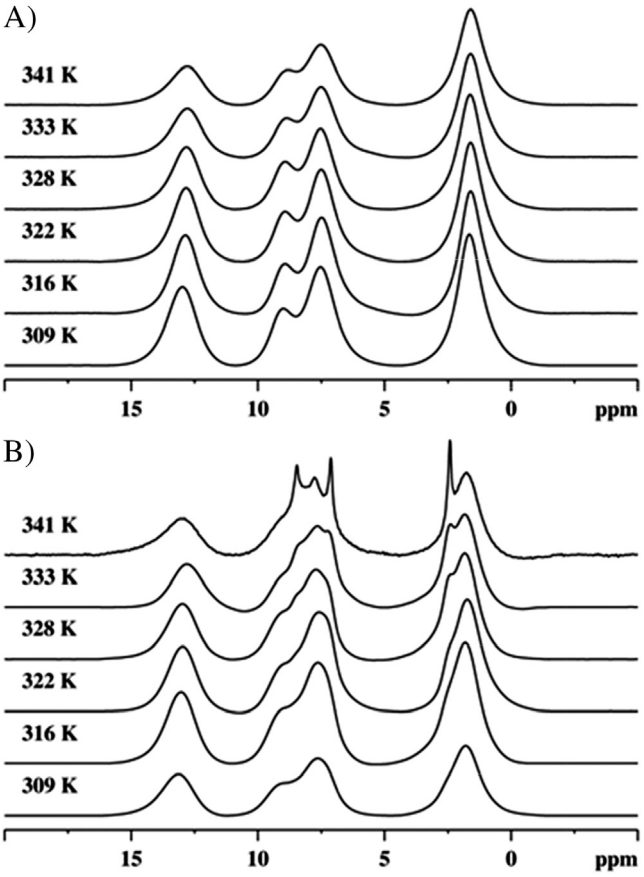

Fig. 5. VT ^{1}H 25 kHz MAS NMR A) IMSA salt and B) IMSA–Teflon composite.

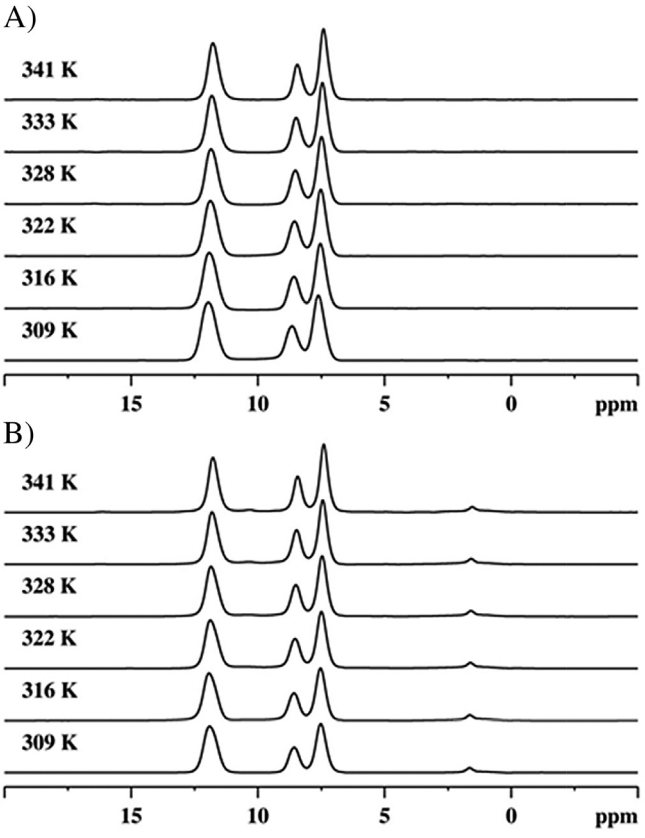

Fig. 6. VT ^{1}H 25 kHz MAS NMR A) IFMS salt and B) IFMS–Teflon composite.

Table 3
T_1 relaxation times for BMSA, IMSA and IFMS salts and composites.

	BMSA	IMSA	IFMS
Salt	5.5 s ± 0.1 s	2.1 s ± 0.1 s	8.1 s ± 0.1 s
Composite	4.5 s ± 0.3 s	0.30 s ± 0.02 ms	5.1 s ± 0.1 s

The IMSA–Teflon composite exhibited a decrease in spin relaxation of 2.1 ± 0.1 s to 0.30 ± 0.01 s, where the difference between salt and membrane is larger than between BMSA and BMSA–Teflon (Table 3). This larger difference is attributed to a more substantial decrease in the strength of dipole–dipole coupling, due to proton dynamics. The activation energy lowered as well from 7.4 ± 0.1 kJ mol^{-1} to 4.0 ± 0.1 kJ mol^{-1}. The activation energy of IMSA–Teflon is significantly lower than BMSA–Teflon composite.

As observed from previous composites, the IFMS–Teflon spin lattice relaxation decreased significantly from pure IFMS salt from 8.1 ± 0.1 s to 5.1 ± 0.1 s as seen in Table 3. The activation energies behaved in with the same trend as previous salts and composites of 5.5 ± 0.6 kJ mol^{-1} and 3.6 ± 0.2 kJ mol^{-1} for IFMS salt and IFMS–Teflon respectively. This composite thus exhibits the lowest activation energy for proton motion, of all of the composites studied here. Comparing this trend in local mobility, as assessed by ^{1}H NMR with bulk properties of charge transport will allow conclusions to be drawn, regarding the proton transport mechanism.

4.5. Proton conductivity

Bulk proton conductivity measurements were conducted between 80 °C and 120 °C under anhydrous conditions. Trends are established between the salts and their composites, and among the pristine salts. All of the pristine salts exhibited proton transport throughout the temperature range of interest with similar conductivities as seen in Fig. 7. The proton conductivities of the composites fall in the range of 10^{-6}–10^{-5} S cm^{-1}, and therefore do not compete with fully hydrated Nafion, which has a proton conductivity 0.1 S cm^{-1}. However at high temperature in anhydrous conditions IFMS–Teflon offers an improvement over Nafion, where Nafion's performance is well-known to plummet under dehydration to 1.5 × 10^{-8} S cm^{-1} or less [7].

Activation energies were obtained for the salts through the Arrhenius plot of proton conductivity were 29.5 ± 1.5, 21.2 ± 0.1 and 29.6 ± 0.8 for BMSA, IMSA and IFMS respectively, as shown in Table 2. Overall, the measured activation energies are higher from bulk proton conductivity measurements as compared to ^{1}H MAS NMR determination of local mobility, as is often observed [24,28]. This is the result of the influence of grain boundaries on long-range conductivity, whereas ^{1}H MAS NMR measures localization motion. Nevertheless, the trends in local dynamics and conductivity are reflected in the salt versus the corresponding composites, where both are observed to increase upon incorporation into the polymer host.

The composites exhibited some variability in their conductivities. Surprisingly, the BMSA–Teflon composite did not exhibit bulk ionic conductivity, although the parent salt had modest H^+ transport. The non-conductive behavior is attributed to the lower salt loading, which was substantially lower than the other two composites. For IMSA–Teflon the proton conductivity is lower than the pristine salt. This could be again due to the packing arrangement within Teflon inhibiting long-range transport due to a low salt loading within the host. Having a low salt content within Teflon reduces the number of charge carriers, and the connectivity within the hydrogen-bonded network, reducing the overall conductivity. This is confirmed by the proton conductivity activation energy for IMSA–Teflon of 29.8 ± 0.9 kJ mol^{-1}, where the increase in activation energy is attributed to incomplete distribution of the salt in the Teflon host that reduced the proton conductivity. This is found for the first two composites, despite indications of enhanced local mobility from the NMR studies described above.

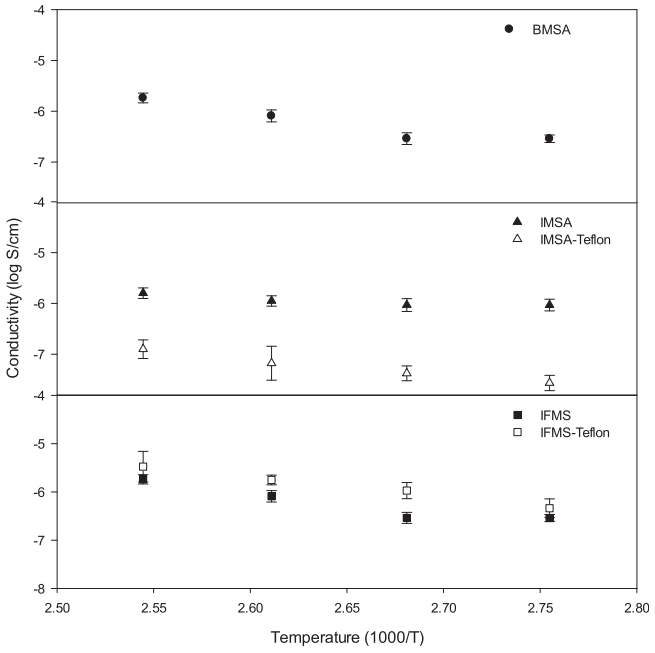

Fig. 7. Proton conductivity data of BMSA, IMSA, IMSA–Teflon, IFMS and IFMS–Teflon under anhydrous conditions, acquired by impedance spectroscopy.

The best performance was measured for the IFMS–Teflon composite. In this case, the conductivity is higher than the pristine salt, which is attributed to the higher salt loading facilitating long-range transport as well as the mechanical support of the host to facilitate proton transport. This is further confirmed by the proton conductivity activation energy of the IFMS–Teflon to 21.4 ± 0.6 kJ mol^{-1} which was lower than the pure salt of 29.6 ± 0.8 kJ mol^{-1}. Thus, for the third composite, the combination of enhanced local dynamics, as revealed by NMR, and sufficient salt loading, resulted in a successful synergy between the salt and the host, and an overall improvement of the long-range ion transport in the resulting material.

5. Conclusion

Solid-state NMR showed that the T_1 relaxation is uniformly decreased when salts are incorporated into a Teflon polymer host. Similarly, the activation energy for local proton mobility, derived from the ^{1}H line-narrowing trends of the hydrogen-bonded proton, decreased when the solid-acid salts were placed into the Teflon framework. Variable temperature ^{1}H DQF NMR depicted higher attenuation of the hydrogen bonded proton in composite form than the salt itself showing that dynamics are increased in the polymer framework. The three pristine solid-acids demonstrated similar bulk proton conductivities, however different conductivities were achieved when inserted into the Teflon membrane support. BMSA–Teflon did not conduct ions, due to the low salt loading that it possessed. IMSA–Teflon conductivity was lower than the pristine salt, again because of the salt loading and packing arrangement in the host. IFMS–Teflon possessed higher conductivity than the salt itself by possessing the highest salt loading and thermal stability and the polymer is facilitating proton transport. These competitive conductivities were achieved in anhydrous conditions.

Acknowledgments

The authors are grateful to Professors A.D. Bain for helpful discussions, to Dr. B. Berno for technical assistance, and to H.F. Gibbs at Brockhouse Institute for Materials Research (BIMR) for acquiring TGA data. This work was funded by the Natural Sciences and Engineering Research Council (NSERC) of Canada.

References

[1] J.J. Baschuk, X. Li, Int. J. Energy Res. 25 (2001) 695.
[2] E.G.G. Services, Fuel Cell Handbook, seventh ed., U.S. Department of Energy, 2004.
[3] K.S. Hwang, M.C. Yang, J. Zhu, J. Grunes, G.A. Somorjai, J. Mol. Catal. A 204 (2003) 499–507.
[4] K.A. Mauritz, R.B. Moore, Chem. Rev. 104 (2004) 4535–4585.
[5] Q. Li, R. He, J.O. Jensen, N.J. Bjerrum, Chem. Mater. 15 (2003) 4896–4915.
[6] D.H. Jung, S.Y. Cho, D.H. Peck, D.R. Shin, J.S. Kim, J. Power Sources 106 (2002) 173–177.
[7] A.V. Anantaraman, C.L. Gardner, J. Electroanal. Chem. 414 (1996) 115–120.
[8] B. Smitha, S. Sridhar, A.A. Khan, J. Membr. Sci. 259 (2005) 10–26.
[9] N. Miyake, J.S. Wainright, R.F. Savinell, J. Electrochem. Soc. 148 (2001) A898–A904.
[10] Y.Y. Shao, G.P. Yin, Z.B. Wang, Y.Z. Gao, J. Power Sources 167 (2007) 235–242.
[11] M.P. Rodgers, J. Berring, S. Holdcroft, Z.Q. Shi, J. Membr. Sci. 321 (2008) 100–113.
[12] S.J. Peighambardoust, S. Rowshanzamir, M. Amjadi, Int. J. Hydrogen Energy 35 (2010) 9349–9384.
[13] M. Susan, A. Noda, S. Mitsushima, M. Watanabe, Chem. Commun. (2003) 938–939.
[14] Z. Peng, A. Morin, P. Huguet, P. Schott, J. Pauchet, J. Phys. Chem. B 115 (2011) 12835–12844.
[15] A. Noda, A.B. Susan, K. Kudo, S. Mitsushima, K. Hayamizu, M. Watanabe, J. Phys. Chem. B 107 (2003) 4024–4033.
[16] S.S. Sekhon, J.S. Park, E. Cho, Y.G. Yoon, C.S. Kim, W.Y. Lee, Macromolecules 42 (2009) 2054–2062.
[17] M. Watanabe, K. Tsurumi, T. Mizukami, T. Nakamura, P. Stonehart, J. Electrochem. Soc. 141 (1994) 2659–2668.
[18] J. Ding, A.G. Fadeev, M. Forsyth, S.A. Forsyth, W. Lu, D.R. MacFarlane, B.R. Mattes, J. Mazurkiewicz, B. Qi, E. Smela, G.M. Spinks, G.G. Wallace, D. Zhou, Science 297 (2002) 983.
[19] S.M. Haile, D.A. Boysen, C.R.I. Chisholm, R.B. Merle, Nature 410 (2001) 910–913.
[20] S.M. Haile, C.R.I. Chisholm, K. Sasaki, D.A. Boysen, T. Uda, Faraday Discuss. 134 (2007) 17.
[21] J.W. Traer, J.F. Britten, G.R. Goward, J. Phys. Chem. B 111 (2007) 5602–5609.
[22] T.O. Peter Atkins, J. Rourke, M. Weller, F. Armstrong, P. Salvador, M. Hagerman, T. Spiro, E. Stiefel, Inorganic Chemistry, fourth ed., W.H. Freeman and Company, New York, 2006.
[23] A.M.A. Martinelli, P. Jacobsson, L. Burjesson, J. Phys. Chem. B 111 (2007).
[24] Z.B. Yan, N.E. De Almeida, J.W. Traer, G.R. Goward, Phys. Chem. Chem. Phys. 15 (2013) 17983–17992.
[25] M.M. Maricq, J.S. Waugh, J. Chem. Phys. 70 (1979) 3300–3316.
[26] N. Chandrakumar, 1D Double Quantum Filter NMR Studies, in: G.A. Webb (Ed.), Annual Reports on NMR Spectroscopy, vol. 67, 2009, pp. 265–329.
[27] S.P. Brown, H.W. Spiess, Chem. Rev. 101 (2001) 4125–4155.
[28] G. Ye, N. Janzen, G.R. Goward, Macromolecules 39 (2006) 3283–3290.
[29] H.C. Torrey, Phys. Rev. 104 (1956) 563–565.
[30] E.L. Hahn, Phys. Rev. 80 (1950) 580–594.
[31] H.A. Every, F. Zhou, M. Forsyth, D.R. MacFarlane, Electrochim. Acta 43 (1998) 1465–1469.
[32] G. Ye, C.A. Hayden, G.R. Goward, Macromolecules 40 (2007) 1529–1537.
[33] X. Yuan, H. Wang, J. Colinsun, J. Zhang, Int. J. Hydrogen Energy 32 (2007) 4365–4380.
[34] T.E. Springer, T.A. Zawodzinski, M.S. Wilson, S. Gottesfeld, J. Electrochem. Soc. 143 (1996) 587–599.
[35] S. Hayashi, K. Hayamizu, Bull. Chem. Soc. Jpn. 64 (1991) 685–687.
[36] R. Freeman, H.D.W. Hill, J. Chem. Phys. 54 (1971) 3367–3377.
[37] Wolfram Research, Inc., Wolfram Research, Inc., Champaign, Illinois, 2010.
[38] G.J.M.P. Vanmoorsel, E.R.H. Vaneck, C.P. Grey, J. Magn. Reson. Ser. A 113 (1995) 159–163.
[39] C. Ochsenfeld, F. Koziol, S.P. Brown, T. Schaller, U.P. Seelbach, F.G. Klarner, Solid State Nucl. Magn. Reson. 22 (2002) 128–153.
[40] J.W. Traer, G.R. Goward, Phys. Chem. Chem. Phys. 12 (2010) 263–272.
[41] H.W. Spiess, Colloid Polym. Sci. 261 (1983) 193–209.
[42] G.R. Goward, M.F.H. Schuster, D. Sebastiani, I. Schnell, H.W. Spiess, J. Phys. Chem. B 106 (2002) 9322–9334.
[43] S.P. Brown, I. Schnell, J.D. Brand, K. Müllen, H.W. Spiess, J. Mol. Struct. 521 (2000) 179–195.
[44] K.D. Kreuer, A. Fuchs, M. Ise, M. Spaeth, J. Maier, Electrochim. Acta 43 (1998) 1281–1288.